

Order-disorder criticality, wetting, and morphological phase transitions in the irreversible growth of far-from-equilibrium magnetic films

Julián Candia^a and Ezequiel V. Albano^b

^a*Departamento de Física, UNLP, CC67,
1900 La Plata, Argentina*

^b*Instituto de Investigaciones Fisicoquímicas Teóricas y Aplicadas
(INIFTA), UNLP, CONICET, Suc.4, CC16,
1900 La Plata, Argentina*

November 8, 2018

Abstract

An exhaustive numerical investigation of the growth of magnetic films in confined $(d + 1)$ -dimensional stripped geometries ($d = 1, 2$) is carried out by means of extensive Monte Carlo simulations. Films in contact with a thermal bath at temperature T , are grown by adding spins having two possible orientations and considering ferromagnetic (nearest-neighbor) interactions. At low temperatures, thin films of thickness L are constituted by a sequence of well-ordered domains of average length $l_D \gg L$. These domains have opposite magnetization. So, the films exhibit “spontaneous magnetization reversal” during the growth process. Such reversal occurs within a short characteristic length l_R , such that $l_D \gg l_R \sim L$. Furthermore, it is found that for $d = 1$ the system is non-critical, while a continuous order-disorder phase transition at finite temperature takes place in the $d = 2$ case. Using standard finite-size scaling procedures, the critical temperature and some relevant critical exponents are determined. Finally, the growth of magnetic films in $(2 + 1)$ dimensions with competing short-range magnetic fields acting along the confinement walls is studied. Due to the antisymmetric condition considered, an interface between domains with spins having opposite orientation develops along the growing direction. Such an interface undergoes a localization-delocalization transition that is the precursor of a wetting transition in the thermodynamic

limit. Furthermore, the growing interface also undergoes morphological transitions in the growth mode. A comparison between the well-studied equilibrium Ising model and the studied irreversible magnetic growth model is performed throughout. Although valuable analogies are encountered, it is found that the nonequilibrium nature of the latter introduces new and rich physical features of interest.

1 Introduction

The preparation and characterization of magnetic nanowires and films is of great interest for the development of advanced microelectronic devices. Therefore, the study of the behavior of magnetic materials in confined geometries, e.g. thin films, has attracted both experimental [1, 2, 3, 4, 5, 6, 7, 8] and theoretical [9, 10, 11, 12, 13] attention. From the theoretical point of view, most of the work has been devoted to the study of equilibrium properties of thin magnetic films [9, 10, 11, 12, 13, 14] and magnetic materials, see e.g. [15, 16, 17, 18]. In contrast, the aim of this work is to study the properties of thin magnetic film growth under far-from-equilibrium conditions, by means of extensive Monte Carlo simulations. Within this context, this work is related to many recent investigations concerned with irreversible growth processes. Indeed, the study of growth systems under far-from-equilibrium conditions is a subject that has drawn great attention during the last decades. Nowadays, this interdisciplinary field has experienced a rapid progress due to its interest in many subfields of physics, chemistry, and even biology, as well as by its relevance in numerous technological applications such as the development of nanoscale devices, polymer science, crystal and polycrystalline growth, gelation, fracture propagation, epidemic spreading, colloids, etc. [19, 20, 21, 22, 23].

For the purpose of studying the properties of thin magnetic film growth under far-from-equilibrium conditions, a variant of the irreversible Eden growth model [24], in which particles are replaced by spins that can adopt two different orientations, is investigated. Our study is performed in confined (stripped) geometries, which resemble recent experiments where the growth of quasi-one-dimensional strips of Fe on a Cu(111) vicinal surface [2] and Fe on a W(110) stepped substratum [8] have been performed. Also, in a related context, the study of the growth of metallic multilayers has shown a rich variety of new physical features. Particularly, the growth of magnetic layers of Ni and Co separated by a Cu spacer layer has recently been studied [25].

The growth of magnetic films with competing short-range magnetic fields, which account for the interaction of the growing films with the substrate, is also investigated in the present work. The competing situation considered leads to rich and complex physical phenomena that exhibit a delicate and subtle interplay between finite-size effects, wetting, and interface growth mechanisms. Besides the technologi-

cal and scientific interest that may arise from the nonequilibrium nature of the model investigated, as already pointed out, this kind of nonequilibrium wetting phenomena also appears closely related to very interesting equilibrium wetting transitions, which have attracted so far considerable experimental and theoretical attention. For instance, surface enrichment and wetting layers have been observed experimentally in a great variety of systems, such as e.g. polymer mixtures [26, 27, 28], adsorption of simple gases on alkali metal surfaces [29, 30, 31], hydrocarbons on mica [32], etc. From the theoretical point of view, the study of wetting transitions at interfaces has been carried out by means of different approaches, such as the mean field Ginzburg-Landau method [33, 34], transfer matrix and Pfaffian techniques [35, 36], density matrix renormalization group methods [37], solving the Cahn-Hilliard equation [38], using Molecular Dynamic simulations [39], solving self-consistent field equations [40], and by means of extensive Monte Carlo simulations [9, 41, 42, 43, 44].

Finally, it should also be remarked that, although the discussion is presented here in terms of a magnetic language, the relevant physical concepts could be extended to other systems such as fluids, polymers, and binary mixtures.

This manuscript is organized as follows: in Section 2 details on the model and the simulation method are given, Section 3 is devoted to the order-disorder critical behavior of magnetic Eden films, Section 4 deals with the study of interfacial phase transitions that arise when competing short-range magnetic fields are considered, while the conclusions are finally stated in Section 5.

2 The model and the simulation method

In the classical Eden model [24] on the square lattice, the growth process starts by adding particles to the immediate neighborhood (the perimeter) of a seed particle. Subsequently, particles are stuck at random to perimeter sites. This growth process leads to the formation of compact clusters with a self-affine interface [20, 21, 22, 23]. The magnetic Eden model (MEM) [45, 46] considers an additional degree of freedom due to the spin of the growing particles. In the present work the MEM is studied in $(d + 1)$ -dimensional rectangular geometries for $d = 1, 2$, as described in [46].

For the case $d = 1$, the MEM is investigated on the square lattice using a rectangular geometry $L \times M$ (with $M \gg L$). The location of each site on the lattice is specified through its rectangular coordinates (i, j) , ($1 \leq i \leq L$, $1 \leq j \leq M$). The starting seed for the growing cluster is a column of parallel-oriented spins placed at $j = 1$ and film growth takes place along the positive longitudinal direction (i.e. $j \geq 2$). Periodic boundary conditions are adopted along the transverse direction. Then, assuming that each spin S_{ij} can be either up or down (i.e. $S_{ij} = \pm 1$), clusters are grown by selectively adding spins to perimeter sites, which are defined as the nearest-neighbor (NN) empty sites of the already occupied ones. Considering a

ferromagnetic interaction of strength $J > 0$ between NN spins, the energy E of a given configuration of spins is given by

$$E = -\frac{J}{2} \sum_{\langle ij, i'j' \rangle} S_{ij} S_{i'j'} \quad , \quad (1)$$

where $\langle ij, i'j' \rangle$ means a summation taken over all occupied NN sites.

Analogously, the MEM in $(2+1)$ dimensions is studied using a $L \times L \times M$ rectangular geometry ($M \gg L$). Each site on the lattice is now identified through the rectangular coordinates (i, j, k) , ($1 \leq i, j \leq L$, $1 \leq k \leq M$), and the starting seed for the growing film is taken to be a plane of $L \times L$ parallel-oriented spins placed at $k = 1$. The energy of the spin configuration is now calculated by extending the summation in Eq.(1) to the three coordinates (i, j, k) . For further details on the MEM defined in rectangular geometries see also [46].

The last part of this paper (see Section 4) is devoted to the study of the $(2+1)$ -dimensional MEM with competing short-range magnetic fields applied along one of the transverse directions. In this case, the periodic boundary conditions along the j -direction are changed to open ones, and competing surface magnetic fields $H > 0$ ($H' = -H$) acting on the sites placed at $j = 1$ ($j = L$) are considered [47]. Then, the energy of a given configuration of spins in this case will be given by

$$E = -\frac{J}{2} \left(\sum_{\langle ijk, i'j'k' \rangle} S_{ijk} S_{i'j'k'} \right) - H \left(\sum_{\langle ik, \Sigma_1 \rangle} S_{i1k} - \sum_{\langle ik, \Sigma_L \rangle} S_{iLk} \right) \quad , \quad (2)$$

where $\langle ijk, i'j'k' \rangle$ means that the summation in the first term is taken over all occupied NN sites, while $\langle ik, \Sigma_1 \rangle$, $\langle ik, \Sigma_L \rangle$ denote summations carried over occupied sites on the surfaces Σ_1 , Σ_L (defined as the $j = 1$ and $j = L$ planes, respectively). Throughout this work we set the Boltzmann constant equal to unity ($k_B \equiv 1$) and consider the absolute temperature, energy, and magnetic fields measured in units of the coupling constant J .

The growth process of a MEM film consists in adding further spins to the growing film taking into account the corresponding interaction energies. A spin is added to the film with a probability proportional to the Boltzmann factor $\exp(-\Delta E/T)$, where ΔE is the total energy change involved. At each step, the probabilities of adding up and down spins to a given site have to be evaluated for all perimeter sites. After proper normalization of the probabilities, the growing site and the orientation of the spin are determined through standard Monte Carlo techniques. Although both the interaction energy (as given either by Eq.(1) or Eq.(2)) and the Boltzmann probability distribution considered for the MEM are similar to those used for the Ising model [9], it must be stressed that these two models operate under extremely different conditions, namely the MEM describes the irreversible growth of a magnetic

material and the Ising model is suitable for the study of a magnetic system under equilibrium conditions. In the MEM, the position and orientation of all deposited spins remain fixed. During the growth process, the system develops a rough growing interface and evolves mainly along the longitudinal direction. Some lattice sites can remain empty even well within the system's bulk, but, since at each growth step all perimeter sites are candidates for becoming occupied, these holes are gradually filled. Hence, far behind the active growing interface, the system is compact and frozen. When the growing interface is close to reaching the limit of the sample, the relevant properties of the irreversibly frozen cluster's bulk (in the region where the growing process has definitively stopped) are computed, the useless frozen bulk is thereafter erased, and finally the growing interface is shifted toward the lowest possible longitudinal coordinate. Hence, repeatedly applying this procedure, the growth process is not limited by the lattice length M . In the present work clusters having up to 10^9 spins have typically been grown.

3 Order-disorder critical behavior of magnetic Eden films

Magnetic Eden films grown on a stripped geometry of finite linear dimension L at low temperatures show an intriguing behavior that we call spontaneous magnetization reversal. In fact, we have observed that long clusters are constituted by a sequence of well ordered magnetic domains of average length $l_D \gg L$. Let l_R be the characteristic length for the occurrence of the spontaneous magnetization reversal. Since $l_R \sim L$, we then conclude that the phenomenon has two characteristic length scales, namely l_D and l_R , such that $l_D \gg l_R \sim L$. Hence, the spontaneous magnetization reversal is essentially due to the small size of the thin film and it becomes irrelevant in the thermodynamic limit. Figure 1 shows a snapshot configuration of the $(1 + 1)$ -dimensional MEM where this phenomenon can be recognized. Here the reversal occurring between a domain of spins up (on the left side) and other one constituted by spins down (on the right), as well as the interface between both domains, can be clearly observed. The magnetization change occurs quite abruptly within the characteristic length $l_R \sim L$. In ordinary thermally driven phase transitions, the system changes from a disordered state at high temperatures to a spontaneously ordered state at temperatures below some critical value T_c , where a second-order phase transition takes place. Regarding the Ising model, one has that, in the absence of an external magnetic field ($H = 0$), the low-temperature ordered phase is a state with non-vanishing spontaneous magnetization ($\pm M_{sp}$). This spontaneous symmetry breaking is possible in the thermodynamic limit only. In fact, it is found

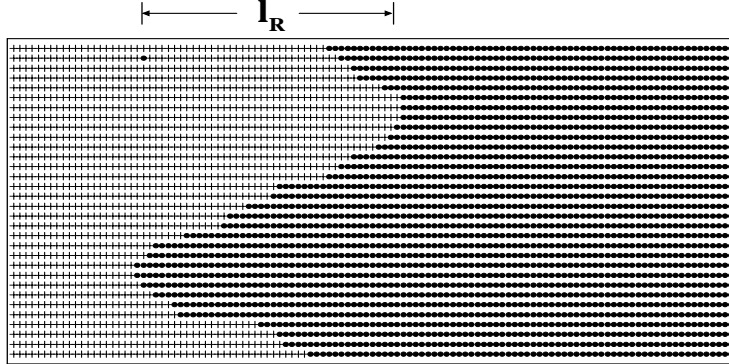


Figure 1: Spontaneous magnetization reversal observed for $L = 32$ and $T = 0.26$ in the $(1+1)$ -dimensional magnetic film. The snapshot configuration shows the collective orientation change: the left (right) domain is constituted by up (down) oriented spins. The snapshot corresponds to the bulk of the sample and the growing interface is not shown. The characteristic length for the occurrence of the magnetization reversal, l_R , is of the order of the lattice width, as marked in the figure.

that the magnetization M of a finite sample formed by N particles, defined by

$$M(T, H = 0) = \frac{1}{N} \sum_{i=1}^N S_i(T, H = 0) \quad , \quad (3)$$

can pass with a finite probability from a value near $+M_{sp}$ to another near $-M_{sp}$, as well as in the opposite direction. Consequently, the magnetization of a finite system, averaged over a sufficiently large observation time, vanishes irrespective of the temperature. That is, the equation $M(T, H = 0) \approx 0$ holds if the observation time (t_{obs}) becomes larger than the ergodic time (t_{erg}), which is defined as the time needed to observe the system passing from $\pm M_{sp}$ to $\mp M_{sp}$. Since Monte Carlo simulations are restricted to finite samples, the standard procedure to avoid the problems treated in the foregoing discussion is to consider the absolute magnetization as an order parameter [48]. Turning back to the MEM, we find that the phenomenon of magnetization reversal also causes the magnetization of the whole cluster to vanish even for very low (but non-zero) temperatures, provided that the film's total length l_F (which plays the role of t_{obs}) is much larger than l_D (which plays the role of t_{erg}). Therefore, as in the case of the Ising model [48], in order to overcome shortcomings derived from the finite-size nature of Monte Carlo simulations we have measured the mean absolute column magnetization, given by

$$|m(j, L, T)| = \frac{1}{L} \left| \sum_{i=1}^L S_{ij} \right| \quad . \quad (4)$$

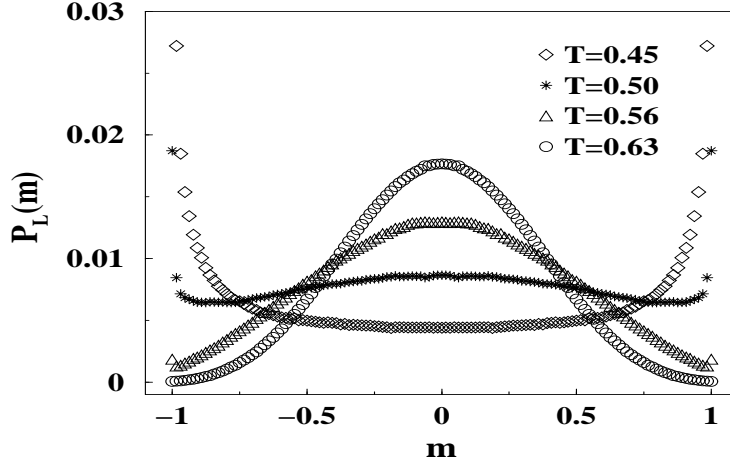


Figure 2: Data corresponding to the $(1+1)$ -dimensional MEM: plots of the probability distribution of the mean column magnetization $P_L(m)$ versus m for the fixed lattice width $L = 128$ and different temperatures, as indicated in the figure. The sharp peaks at $m = \pm 1$ for $T = 0.45$ have been truncated, in order to allow a detailed observation of the plots corresponding to higher temperatures. This behavior resembles that of the one-dimensional Ising model.

It is found that $|m(j; L, T)|$ exhibits a transient growing period with a characteristic length of order L , followed by the attainment of a stationary regime, which is independent of the orientation of the seed.

The mean column magnetization given by Eq.(4) is a fluctuating quantity that can assume $L + 1$ values. Then, for given values of both L and T , the probability distribution of the mean column magnetization ($P_L(m)$) can straightforwardly be evaluated, since it represents the normalized histogram of m taken over a sufficiently large number of columns in the stationary region [49, 50, 51]. In the thermodynamic limit ($L \rightarrow \infty$) the probability distribution ($P_\infty(m)$) of the order parameter of an equilibrium system at criticality is universal (up to re-scaling of the order parameter) and thus it contains very useful and interesting information on the universality class of the system [52, 53, 54]. For example, $P_L(m)$ contains information about all momenta of the order parameter m , including universal ratios such as the Binder cumulant [52].

Figure 2 shows the thermal dependence of $P_L(m)$ versus m , as obtained for the $(1+1)$ -dimensional MEM. We can observe that at high temperatures $P_L(m)$ is a Gaussian centered at $m = 0$. As the temperature gets lowered, the distribution broadens and develops two peaks at $m = \pm 1$. Further decreasing the temperature causes these peaks to become dominant while the distribution turns distinctly non-Gaussian, exhibiting a minimum just at $m = 0$. It should be pointed out that the

emergence of the maxima at $m = \pm 1$ is quite abrupt. This behavior reminds us the order parameter probability distribution characteristic of the one-dimensional Ising model. In fact, for the well studied d -dimensional Ising model [51, 55], we know that for $T > T_c$, $P_L(M)$ [56] is a Gaussian centered at $M = 0$, given by

$$P_L(M) \propto \exp\left(\frac{-M^2 L^d}{2T\chi}\right) , \quad (5)$$

where the susceptibility χ is related to order parameter fluctuations by

$$\chi = \frac{L^d}{T} \left(\langle M^2 \rangle - \langle M \rangle^2 \right) . \quad (6)$$

Decreasing the temperature, the order parameter probability distribution broadens, it becomes non-Gaussian, and near T_c it splits into two peaks that get the more separated the lower the temperature. For $T < T_c$ and linear dimensions L much larger than the correlation length ξ of order parameter fluctuations, one may approximate $P_L(M)$ near the peaks by a double-Gaussian distribution, i.e.

$$P_L(M) \propto \exp\left(\frac{-(M - M_{sp})^2 L^d}{2T\chi}\right) + \exp\left(\frac{-(M + M_{sp})^2 L^d}{2T\chi}\right) , \quad (7)$$

where M_{sp} is the spontaneous magnetization, while the susceptibility χ is now given by

$$\chi = \frac{L^d}{T} \left(\langle M^2 \rangle - \langle |M| \rangle^2 \right) . \quad (8)$$

From Eq.(5) it turns out that the Gaussian squared width σ^2 associated with high temperature distributions is very close to the 2nd moment of the order parameter, i.e.

$$\sigma^2 \approx \langle M^2 \rangle . \quad (9)$$

It should be noticed that this equation is a straightforward consequence of the Gaussian shape of the order parameter probability distribution and, thus, it holds for the MEM as well. From the well known one-dimensional exact solution for a chain of L spins [57] one can establish the relationship

$$\chi = \frac{1}{T} \exp(2/T) ; \quad (10)$$

then, Eqs.(6) and (10) lead us to

$$\langle M^2 \rangle = \frac{1}{L} \exp(2/T) \quad (11)$$

(where it has been taken into account that $\langle M \rangle = 0$ due to finite-size effects, irrespective of temperature). From Eqs.(9) and (11) we can see that the high-temperature

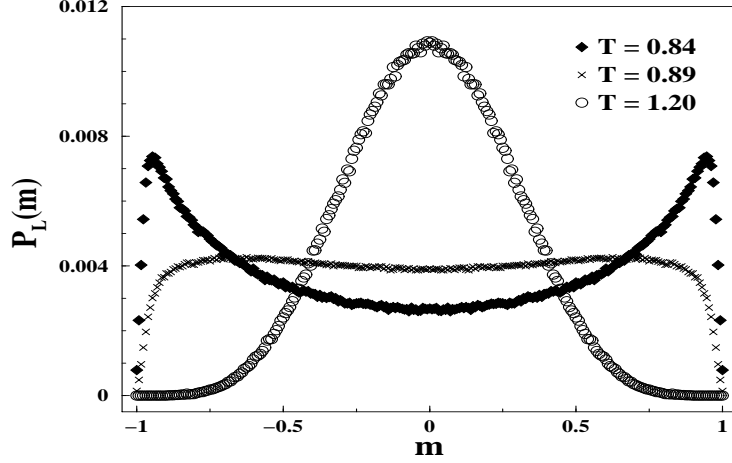


Figure 3: Data corresponding to the $(2 + 1)$ –dimensional MEM: plots of the probability distribution $P_L(m)$ versus m for the fixed lattice size $L = 16$ and different temperatures, as indicated in the figure. The occurrence of two maxima located at $m = \pm M_{sp}$ (for a given value of M_{sp} such that $0 < M_{sp} < 1$) is the hallmark of a thermal continuous phase transition that takes place at a finite critical temperature.

Gaussian probability distribution broadens exponentially as T gets lowered, until it develops delta-like peaks at $M = \pm 1$ as a consequence of a boundary effect on the widely extended distribution. It should be noted that for $d \geq 2$ this phenomenon is prevented by the finite critical temperature which splits the Gaussian, as implied by Eq.(7).

Figure 3 shows the thermal evolution of the probability distribution as obtained for the $(2 + 1)$ –dimensional MEM. Notice that now m is defined by an average over transverse planes constituted by $L \times L$ spins, analogously to Eq.(4). Hence, m takes now $L^2 + 1$ possible values. For high temperatures, the probability distribution corresponds to a Gaussian centered at $m = 0$. At lower temperatures we observe the onset of two maxima located at $m = \pm M_{sp}$ ($0 < M_{sp} < 1$), which become sharper and approach $m = \pm 1$ as T is gradually decreased. These low-temperature probability distributions clearly reflect the occurrence of the magnetization reversal effect already discussed for the case of $(1 + 1)$ –dimensional magnetic films.

Figure 4 shows the location of the maximum of the probability distribution as a function of temperature for both $(d + 1)$ –dimensional MEM models (with $d = 1, 2$), where only maxima located at $m \geq 0$ are considered, since the distributions are symmetric around $m = 0$. After inspection of figure 4, it becomes apparent the different qualitative behavior of both systems. Indeed, while for the $d = 2$ case we observe a smooth transition from the $m_{max} = 0$ value characteristic of high temperatures to nonzero m_{max} values that correspond to lower temperatures, the

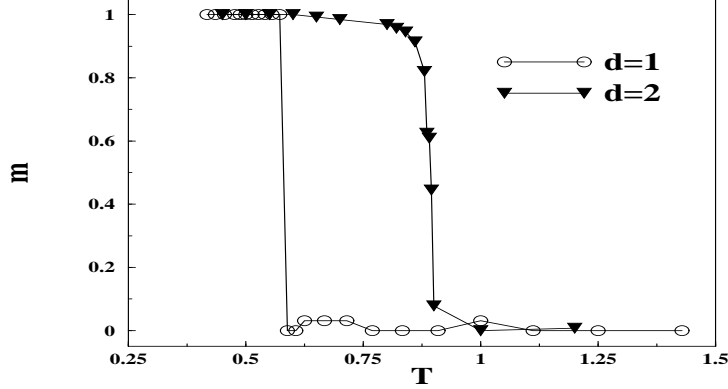


Figure 4: Plots showing the location of the maximum of the probability distribution as a function of temperature for both $(d + 1)$ -dimensional MEM models ($d = 1, 2$). The lines are guides to the eye. The smooth transition for $d=2$ is the signature of a thermal continuous phase transition occurring at a finite critical temperature.

curve obtained for $d = 1$ shows instead a Heaviside-like jump. In contrast to the $(1 + 1)$ -dimensional case, the behavior exhibited by the $(2 + 1)$ -dimensional MEM (e.g. as displayed by figures 3 and 4) is the signature of a thermal continuous phase transition that takes place at a finite critical temperature.

From the finite-size scaling theory, developed for the treatment of finite-size effects at criticality and under equilibrium conditions [58, 59], it is well known that if a thermally driven phase transition occurs at a temperature $T_c > 0$ in the thermodynamic limit, then in a confined geometry of linear dimension L this transition becomes smeared out over the temperature region $\Delta T(L)$ around a shifted effective transition temperature $T_c(L)$, which are related to L through phenomenological exponents. Indeed, it is found that

$$\Delta T(L) \propto L^{-\theta} \quad (12)$$

and

$$|T_c(L) - T_c| \propto L^{-\lambda} \quad , \quad (13)$$

where the rounding and shift exponents are given by $\theta = \lambda = \nu^{-1}$, respectively, and where ν is the exponent that characterizes the divergence of the correlation length at criticality.

Furthermore, from well-established finite-size scaling relations, the following Ansätze hold just at criticality:

$$\langle |m(L, T = T_c)| \rangle \propto L^{-\beta/\nu} \quad (14)$$

and

$$\chi_{max}(L) \propto L^{\gamma/\nu} \quad , \quad (15)$$

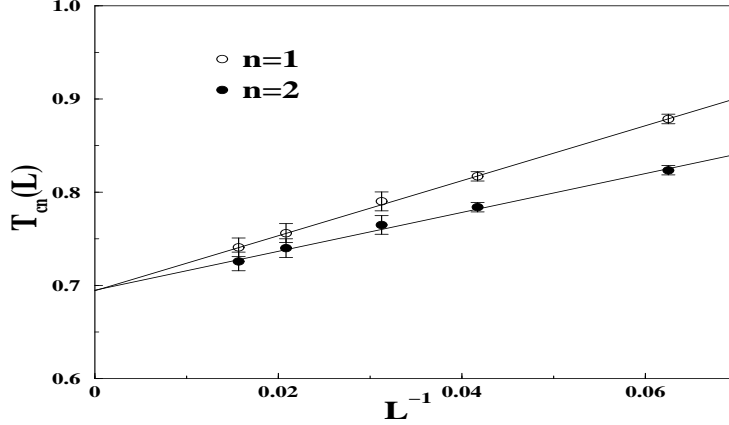


Figure 5: Plots of the effective finite-size critical temperatures $T_{cn}(L)$ versus L^{-1} (for $n = 1, 2$) corresponding to the $(2 + 1)$ -dimensional magnetic film. $T_{c1}(L)$ is defined as the value that corresponds to $\langle |m| \rangle = 0.5$, while $T_{c2}(L)$ is the temperature that corresponds to the maximum of the susceptibility. The solid lines show the linear extrapolations that meet at the critical point given by $T_c = 0.69 \pm 0.01$.

where β and γ are the order parameter and the susceptibility critical exponents, respectively. Note that $\chi_{max}(L)$, as given by Eq.(15), refers to the maximum of $\chi(L, T)$ as a function of T for a fixed lattice size L .

In order to describe quantitatively the critical behavior of the MEM in $(2 + 1)$ -dimensions, we may test the validity of the scaling relations given in Eqs.(12)-(15). As in the case of equilibrium systems, in the present case various “effective” L -dependent critical temperatures can also be defined. In particular, we will define $T_{c1}(L)$ as the value that corresponds to $\langle |m| \rangle = 0.5$ for fixed L , and $T_{c2}(L)$ as the one corresponding to the maximum of the susceptibility for a given L , assuming that the susceptibility is related to order parameter fluctuations in the same manner as for equilibrium systems (as given by Eqs.(6) and (8)). Then, T_c can be obtained from plots of $T_{cn}(L)$ versus L^{-1} (for $n = 1, 2$), as is shown in figure 5. Following this procedure we find that both $T_{c1}(L)$ and $T_{c2}(L)$ extrapolate (approximately) to the same value, allowing us to evaluate the critical temperature $T_c = 0.69 \pm 0.01$ in the thermodynamic limit.

After determining T_c , the correlation length exponent ν can be evaluated by means of Eq.(13), making the replacement $\lambda = 1/\nu$. Indeed, taking T_c at the mean, maximum and minimum values allowed by the error bars, we obtain six log-log plots of $|T_{cn}(L) - T_c|$ versus L for $n = 1, 2$. The slope of each of these plots, not shown here for the sake of space, yields a value for ν . The obtained values are:

$$\nu = 1.08 \quad (T_c = 0.68), \quad \nu = 1.00 \quad (T_c = 0.69),$$

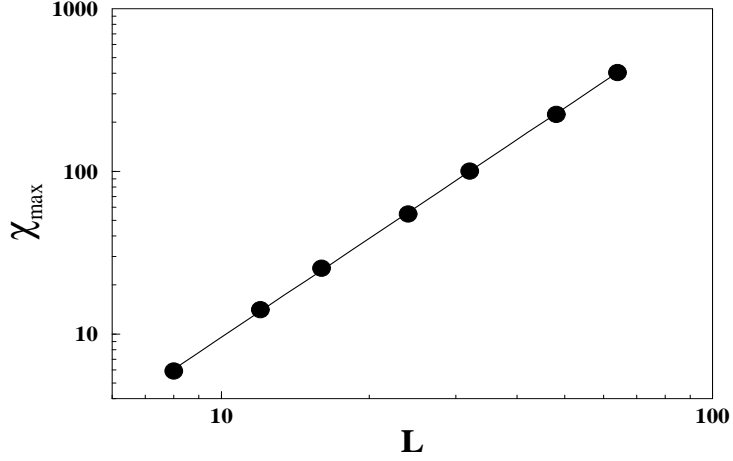


Figure 6: Log-log plot of χ_{max} versus L . The linear fit (solid line) yields $\gamma/\nu = 2.02 \pm 0.04$.

$$\nu = 0.88 \quad (T_c = 0.70) \quad \text{for } n = 1, \quad (16)$$

and

$$\begin{aligned} \nu &= 1.20 \quad (T_c = 0.68), \quad \nu = 1.08 \quad (T_c = 0.69), \\ \nu &= 0.95 \quad (T_c = 0.70) \quad \text{for } n = 2. \end{aligned} \quad (17)$$

Thus our estimate is given by $\nu = 1.04 \pm 0.16$, where the error bars reflect the error derived from the evaluation of T_c , as well as the statistical error.

Studying the susceptibility χ as a function of the temperature for several different lattice sizes, it is found that χ exhibits a peak, which becomes sharper and shifts toward lower temperatures as L is increased. Hence, Eq.(15) can be used to evaluate γ/ν from the slope of a log-log plot of χ_{max} versus L , as figure 6 shows. The linear fit yields $\gamma/\nu = 2.02 \pm 0.04$. Using this value and the value formerly obtained for ν we thus determine $\gamma = 2.10 \pm 0.36$.

Figure 7 shows log-log plots of $\langle |m| \rangle (T = T_c)$ versus L for the mean, maximum and minimum allowed values of T_c . Considering only the larger lattices, the linear fits to the data according to Eq.(14) yield the following estimates: $\beta/\nu = 0.11$, $\beta/\nu = 0.16$ and $\beta/\nu = 0.19$. We then assume the value $\beta/\nu = 0.15 \pm 0.04$, where the error bars reflect the error derived from the evaluation of T_c , as well as the statistical error. From this value and the value formerly obtained for ν we thus determine $\beta = 0.16 \pm 0.05$.

In this manner, we conclude that magnetic Eden films grown on stripped $(d+1)$ -dimensional geometries are non-critical for $d = 1$, in the sense that the ordered phase is trivially found only at $T = 0$. However, MEM films exhibit a continuous order-disorder phase transition at the critical temperature $T_c = 0.69 \pm 0.01$ for $d = 2$.

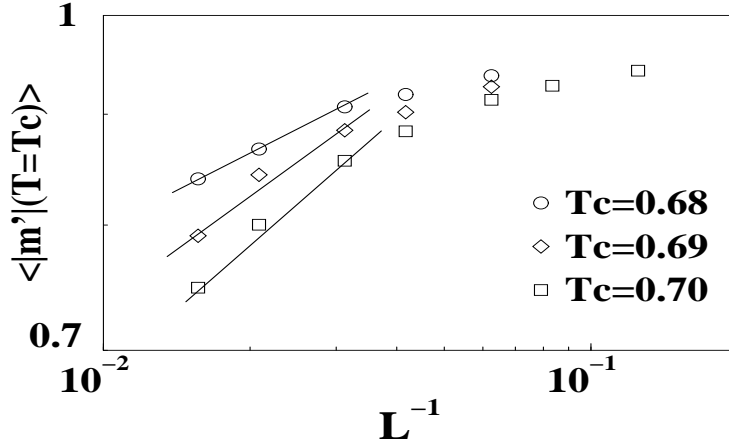


Figure 7: Log-log plots of average magnetization measured at the critical point $\langle m(T = T_c) \rangle$ versus L^{-1} as obtained for the mean, maximum and minimum allowed values of T_c . The linear fits (solid lines) yield an estimate $\beta/\nu = 0.16 \pm 0.05$.

Furthermore, the critical exponents of the MEM in $(2 + 1)$ dimensions, as obtained using a finite-size scaling analysis, are: $\nu = 1.04 \pm 0.16$, $\gamma = 2.10 \pm 0.36$, and $\beta = 0.16 \pm 0.05$.

4 Study of the $(2 + 1)$ -dimensional MEM with competing short-range magnetic fields: Wet-ting and morphological phase transitions

In this section, we will study the interfacial phase transitions that arise in the $(2+1)$ -dimensional MEM, when competing short-range magnetic fields applied along one of the transverse directions are considered. As described in Section II, we will assume competing surface magnetic fields $H > 0$ ($H' = -H$) acting on the surfaces $j = 1$ and $j = L$. Hence, the energy associated to a given spin configuration acquires an additional term due to the interaction of the surface spins with the applied magnetic fields (see Eq.(2)).

As shown in figure 8, magnetic Eden films that grow in a confined geometry with competing surface fields exhibit a very rich phase diagram, which is composed of eight regions. These regions are delimited by several distinct, well-defined transition curves. As will be shown below, the bulk order-disorder (finite-size) critical point $T_c(L)$, the Ising-like quasi-wetting transition curve $T_w(L, H)$, and two morphological transitions associated to the curvature of the growing interface (namely, from convex to non-defined to concave), can be quantitatively located. Moreover, in or-

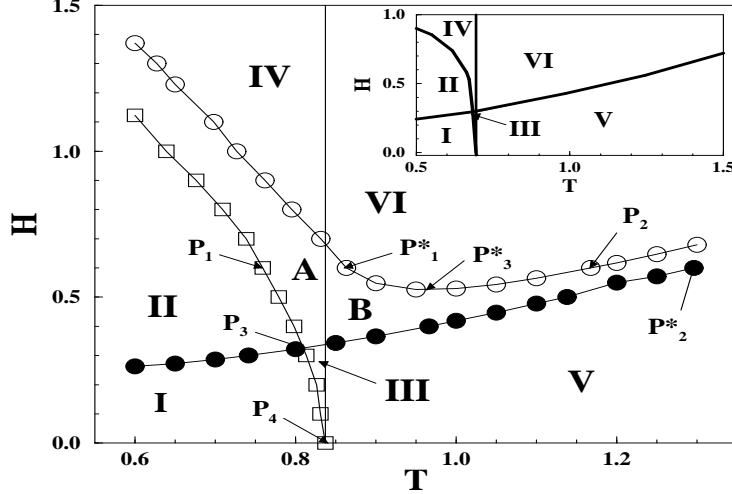


Figure 8: $H - T$ phase diagram corresponding to a lattice of size $L = 12$. The vertical straight line at $T_c(L) = 0.84$ corresponds to the L -dependent critical temperature, which separates the low-temperature ordered phase from the high-temperature disordered phase. Open (filled) circles refer to the transition between non-defined and concave (convex) growth regimes, and squares stand for the Ising-like localization-delocalization transition curve. Eight different regions are distinguished, as indicated in the figure. Also indicated are seven representative points that are discussed in the text. The inset shows the phase diagram corresponding to the thermodynamic limit composed of six different regions.

der to gain some insight into the physics involved in this complex phase diagram, some typical snapshot configurations characteristic of the various different growth regimes are obtained (see figure 9) and discussed. Finally, the phase diagram in the thermodynamic limit will be drawn (see inset of figure 8) by extrapolating finite-size results (see figure 10).

The (L -dependent) bulk order-disorder critical temperature can be identified with the peak of the susceptibility at zero surface field. For $L = 12$, the critical point so defined is $T_c(L = 12) = 0.84$, and is shown in figure 8 by a vertical straight line. So, the left (right) hand side part of the phase diagram corresponds to the ordered (disordered) growth regime that involves Regions I, II, III, IV , and A (Regions V, VI , and B).

Using a standard procedure [9], the localization-delocalization transition curve (on the $H - T$ plane) corresponding to the up-down interface running along the walls can be computed, considering that a point with coordinates (H_w, T_w) on this curve maximizes $\chi(H, T)$. So, the size-dependent localization-delocalization transition curve is obtained, as shown in figure 8 (open squares). As in the case of the Ising

model, this quasi-wetting transition refers to a transition between a nonwet state that corresponds to a localized interface bound to one of the confinement walls, and a wet state associated with a delocalized domain interface centered between roughly equal domains of up and down spins. The localization-delocalization transition in a confined system is indeed the precursor of the true wetting transition, which occurs in the thermodynamic limit [9, 34, 41]. In fact, there is observed a finite jump in the wetting layer thickness that takes place as a result of the finite size of the system. As the lattice size is increased, the magnitude of the jump grows and diverges in the $L \rightarrow \infty$ limit, as expected for a continuous wetting transition.

Since the MEM is a nonequilibrium kinetic growth model, it also allows the identification of another kind of phase transition, namely a morphological transition associated with the curvature of the growing interface of the system. To avoid confusion, we would like to remark that the term *interface* is used here for the transverse interface between occupied and empty lattice sites, while it was used above for the longitudinal interface between up and down spin domains. To explore this phenomenon quantitatively, the behavior of the contact angles between the growth interface and the confinement walls (as functions of temperature and magnetic field) have to be investigated. Clearly, two different contact angles should be defined in order to locate this transition, namely θ_D for the angle corresponding to the dominant spin cluster, and θ_{ND} for the one that corresponds to the non-dominant spin cluster. Both contact angles can straightforwardly be determined by measuring the location of the growth interface averaged over a sufficiently long growing time. In this way, three different growth regimes can be distinguished: (i) the concave growth regime that occurs when the system partially wets the walls on both sides (i.e. for $\theta_D, \theta_{ND} < \frac{\pi}{2}$), (ii) the convex growth regime that occurs for $\theta_D, \theta_{ND} > \frac{\pi}{2}$, and (iii) the regime of non-defined curvature that occurs otherwise. The corresponding transition curves obtained for confined magnetic Eden films are shown on the $H - T$ phase diagram of figure 8, where open (filled) circles refer to the transition between non-defined and concave (convex) growth regimes.

As anticipated above, we will now introduce and discuss some characteristic snapshot pictures, in order to provide qualitative explanations that account for the different growth regimes observed. Let us begin with Region *I* (see figure 8), that corresponds to the Ising-like nonwet state and the convex growth regime. In this region, the temperature is low and the system grows in an ordered state, i.e. the dominant spin domain prevails and the deposited particles tend to have their spins all pointing in the same direction. Small clusters with the opposite orientation may appear preferably on the surface where the non-dominant orientation field is applied. These “drops” might grow and drive a magnetization reversal, thus changing the sign of the dominant domain. Indeed, the formation of sequences of well-ordered domains are characteristic of the ordered phase of confined (finite-size) spin systems such as the Ising magnet [9]. Due to the open boundary conditions, perimeter sites

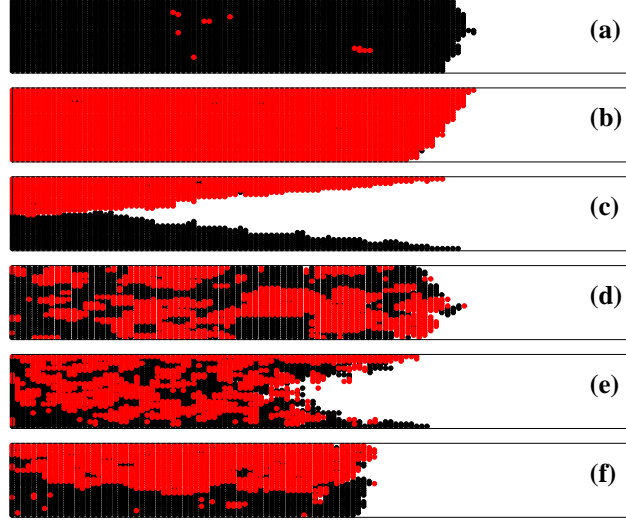


Figure 9: Snapshot pictures showing a longitudinal slice given by a fixed value of the transverse coordinate i . Grey (black) points correspond to spins up (down). The surface field on the upper (lower) confinement wall is positive (negative). The snapshots correspond to a lattice size $L = 32$ and several different values of temperature and surface fields: (a) $H = 0.05$, $T = 0.6$; (b) $H = 0.5$, $T = 0.55$; (c) $H = 1.4$, $T = 0.6$; (d) $H = 0.1$, $T = 1.0$; (e) $H = 1.6$, $T = 1.4$; and (f) $H = 0.20$, $T = 0.82$.

at the confinement walls experience a missing neighbor effect, that is, the number of NN sites is lower than for the case of perimeter sites on the bulk. Since H is too weak to compensate this effect, the system grows preferentially along the center of the sample as compared to the walls, and the resulting growing interface exhibits a convex shape. So, Region *I* corresponds to the Ising-like nonwet state and the convex growth regime. A typical snapshot configuration characteristic of Region *I* is shown in figure 9(a).

Let us now consider an increase in the surface magnetic fields, such as the system may be driven into Region *II* (see figure 8). Since the temperature is kept low, the system is still in its ordered phase and neighboring spins grow preferably parallel-oriented. The surface fields in this region are stronger and thus capable of compensating the missing NN sites on the surfaces. But, since the fields on both surfaces have opposite signs, it is found that, on the one hand, the field that has the same orientation as the dominant spin cluster favors the growth of surface spins, while on the other hand, the sites on the surface with opposite field have a lower probability to be chosen during the growth process. Hence, the contact angle corresponding to the dominant spin cluster is then $\theta_D < \frac{\pi}{2}$, while the non-dominant is $\theta_{ND} > \frac{\pi}{2}$. Thus, on the disfavored side the growing interface becomes pinned and the curvature of the growing interface is not defined. Figure 9(b) shows a typical

snapshot corresponding to Region *II*.

Keeping H fixed within Region *II* but increasing the temperature, thermal noise will enable the formation of drops on the disfavored side that eventually may nucleate into larger clusters as the temperature is increased even further. This process may lead to the emergence of an up-down interface, separating oppositely oriented domains, running in the longitudinal direction (i.e. parallel to the walls). Since sites along the up-down interface are surrounded by oppositely oriented NN spins, they have a low growing probability. So, in this case the system grows preferably along the confinement walls and the growing interface is concave (figure 9(c)). Then, as the temperature is increased, the system crosses to Region *A* (see figure 8) and the onset of two competitive growth regimes is observed, namely: *(i)* one exhibiting a non-defined growing curvature that appears when a dominant spin orientation is present, as in the case shown in figure 9(b); *(ii)* another that appears when an up-down interface is established and the system has a concave growth interface, as is shown in figure 9(c).

On further increasing the temperature and for large enough fields, the formation of a stable longitudinal up-down interface that pushes back the growing interface is observed. So, the system adopts the concave growth regime (see figure 9(c) corresponding to Region *IV* in figure 8). Increasing the temperature beyond $T_c(L)$, a transition from a low-temperature ordered state (Region *IV*) to a high-temperature disordered state (Region *VI*, see figure 9(e)), both within the concave growth regime, is observed. Analogously, for small enough fields, a temperature increase drives the system from the ordered convex growth regime (Region *I*) to the disordered convex growth regime (Region *V*, see figure 9(d)). As shown in figure 8, there is also an intermediate fluctuating state (Region *B*) between Regions *V* and *VI*, characterized by the competition between the disordered convex growth regime and the disordered concave one.

Finally, a quite unstable and small region (Region *III* in figure 8) that exhibits the interplay among the growth regimes of the contiguous regions, can also be identified. Since the width of Region *III* is of the order of the rounding observed in $T_c(L)$, large fluctuations between ordered and disordered states are observed, as well as from growth regimes of non-defined curvature to convex ones. However, figure 9(f) shows a snapshot configuration that is the fingerprint of Region *III*, that may prevail in the thermodynamic limit, namely a well defined spin up-down interface with an almost flat growing interface.

Let us now extrapolate our results to show that the rich variety of phenomena found in a confined geometry is still present in the thermodynamic limit ($L \rightarrow \infty$), leading to the phase diagram shown in the inset of figure 8. As clearly seen by comparison with the finite-size results, the crossover Regions *A* and *B* collapse in this limit, so only the six regions that correspond to well identified growth regimes (as illustrated by the snapshot configurations of figure 9) appear to remain.

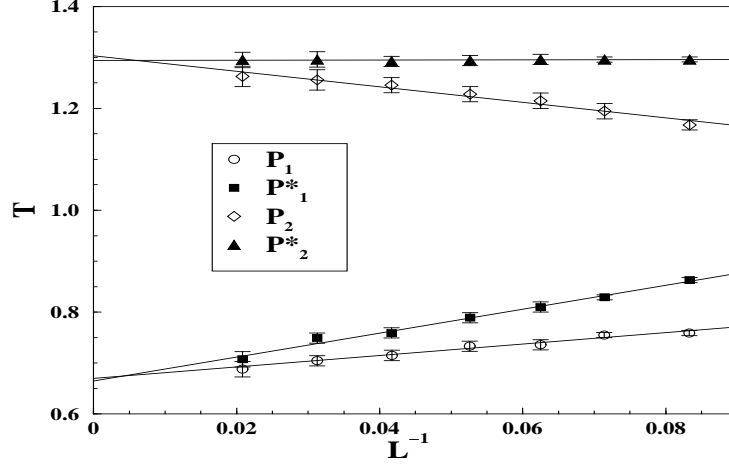


Figure 10: Plots of T versus L^{-1} for $12 \leq L \leq 48$, corresponding to the points P_1, P_1^*, P_2 , and P_2^* , all of them with $H = 0.6$. The fits to the data (solid lines) show that, within error bars, $P_i \rightarrow P_i^*$ ($i = 1, 2$) for $L \rightarrow \infty$.

In order to illustrate the extrapolation procedure, the following seven representative points of the finite-size phase diagram are discussed in detail: (i) the points labeled P_1, P_1^*, P_2 , and P_2^* , that correspond to the intersections of the $H = 0.6$ line with the various transition curves shown in figure 8, and (ii) the points labeled P_3, P_3^* , and P_4 , that refer to the intersection point between Regions *I, II, III*, and *A*, the minimum of the limiting curve between Regions *IV-VI* and *A-B*, and the zero-field transition point, respectively.

Figure 10 shows plots of T versus L^{-1} for $12 \leq L \leq 48$ corresponding to the points P_1, P_1^*, P_2 , and P_2^* . Also shown in the figure are the fits to the data extrapolated to $L^{-1} = 0$. The results from the extrapolations are: $T_1 = 0.67 \pm 0.01$, $T_1^* = 0.66 \pm 0.01$, and $T_2 = 1.30 \pm 0.02$, $T_2^* = 1.29 \pm 0.01$, pointing out that, within error bars, $P_i \rightarrow P_i^*$ ($i = 1, 2$) in the $L \rightarrow \infty$ limit. Using the same procedure, the extrapolations of P_3 and P_3^* (not shown here) give: $H_3 = 0.30 \pm 0.01$, $H_3^* = 0.31 \pm 0.02$, and $T_3 = 0.69 \pm 0.01$, $T_3^* = 0.71 \pm 0.03$. So, one has $P_3 \rightarrow P_3^*$ for $L \rightarrow \infty$ within error bars. Finally, the extrapolation of P_4 is $T_4 = T_c = 0.69 \pm 0.01$.

Using the above-mentioned extrapolation procedure, the phase diagram in the thermodynamic limit can be drawn, as shown in the inset of figure 8. By comparison with the finite-size phase diagram of figure 8, one can note that, as anticipated, the crossover Regions *A* and *B* appear in the phase diagram just as a consequence of the finite-size nature of confined geometries, since they collapse in the $L \rightarrow \infty$ limit. Moreover, we conjecture that Region *III* may remain in the thermodynamic limit. Although this (very tiny!) region corresponds to a physically well-characterized growth regime, since one expects that the system in this region may grow in an

ordered phase with a delocalized up-down domain interface and a convex growing interface, statistical errors due to large fluctuations close to criticality hinder a more accurate location of this region. The unambiguous clarification of our conjecture remains as an open question that will require a huge computational effort.

Besides an Ising-like continuous wetting transition, coupled morphological transitions in the growing interface, which arise from the MEM's kinetic growth process, have also been identified. Comparing the equilibrium wetting phase diagram of the Ising model [9, 33, 41] and that of the MEM, it follows that the nonequilibrium nature of the latter introduces new and rich physical features of interest: the non-wet (wet) Ising phase splits out into Regions *I* and *II* (Regions *III* and *IV*), both within the ordered regime ($T < T_c$) but showing an additional transition in the interface growth mode. Also, the disordered state of the Ising system ($T > T_c$) splits out into Regions *V* and *VI* exhibiting a transition in the interface growth mode.

5 Conclusions

In the present work we have studied the growth of magnetic Eden films with ferromagnetic interactions between nearest-neighbor spins in a $(d + 1)$ -dimensional rectangular geometry (for $d = 1, 2$), by means of extensive Monte Carlo simulations. For both dimensions the phenomenon of spontaneous magnetization reversal is observed at low temperatures. Indeed, MEM films grown at low temperatures are constituted by a sequence of magnetic domains, each of them with a well-defined magnetization, such that the magnetization of adjacent domains is antiparallel. Furthermore, it is found that the $(1 + 1)$ -dimensional MEM is non-critical, while the $(2 + 1)$ -dimensional MEM undergoes a thermally driven second-order phase transition at finite temperature, which is evaluated by extrapolating some “effective” L -dependent critical temperatures to the thermodynamic limit ($L \rightarrow \infty$). Using a finite-size scaling theory, some relevant critical exponents that characterize the behavior of the $(2 + 1)$ -dimensional MEM at criticality are determined. The observed behavior is reminiscent to that of the equilibrium Ising model, although it should be stressed that the MEM is a far-from-equilibrium growing system.

Finally, the $(2 + 1)$ -dimensional MEM with competing surface magnetic fields, which may account for the interaction of the growing magnetic films with the substrate, is investigated. An Ising-like localization-delocalization wetting transition and, on the other hand, a morphological transition associated with the curvature of the growing interface, are located. In this way, eight different regions on the $H - T$ phase diagram for a finite-size lattice are identified. Moreover, the characteristic behavior of typical growth processes within each region are discussed, and qualitative explanations that account for the observed features are provided. Extrapolating the results obtained for various lattice sizes, the phase diagram corresponding to the

$L \rightarrow \infty$ limit is also determined. It is composed of six different regions, since two crossover regions identified in the finite-size phase diagram appear to collapse in the thermodynamic limit. The phase diagram obtained shows new and rich physical features of interest, which arise as a consequence of the nonequilibrium nature of the model investigated.

We expect that the present study will contribute to the fields of irreversible growth processes in confined geometries and nonequilibrium wetting phenomena, and we hope that it will stimulate further experimental and theoretical work in these topics of widespread technological and scientific interest.

ACKNOWLEDGMENTS. Work supported by CONICET, UNLP, and AN-PCyT (Argentina).

References

- [1] U. Gradmann, J. Magn. Magn. Mater. **100**, 481 (1991).
- [2] J. Shen et al., Phys. Rev. B **56**, 2340 (1997).
- [3] J. Hauschild, U. Gradmann, and H.J. Elmers, Appl. Phys. Lett. **72**, 3211 (1998).
- [4] C.-Y. Hong, H.-E. Horng, F.C. Kuo, S.Y. Yang, H.C. Yang, and J.M. Wu, Appl. Phys. Lett. **75**, 2196 (1999).
- [5] J. Shen, A.K. Swan, and J.F. Wendelken, Appl. Phys. Lett. **75**, 2987 (1999).
- [6] J.-S. Tsay and Y.-D. Yao, Appl. Phys. Lett. **74**, 1311 (1999).
- [7] H.J. Elmers, J. Hauschild, and U. Gradmann, Phys. Rev. B **59**, 3688 (1999).
- [8] O. Pietzsch, A. Kubetzka, M. Bode, and R. Wiesendanger, Phys. Rev. Lett. **84**, 5212 (2000).
- [9] E.V. Albano, K. Binder, D.W. Heermann, and W. Paul, Surf. Sci. **223**, 151 (1989).
- [10] D.P. Landau and K. Binder, J. Magn. Magn. Mater. **104**, 841 (1992).
- [11] D. Karevski and M. Henkel, Phys. Rev. B **55**, 6429 (1997).
- [12] J.T. Ou, F. Wangand, and D.L. Lin, Phys. Rev. E **56**, 2805 (1997).
- [13] F.D.A. Aarão Reis, Phys. Rev. B **58**, 394 (1998); **62** 6565 (2000).

- [14] M. L. Rubio Puzzo and E. V. Albano, J. Magn. Magn. Mater. **241**, 110 (2002).
- [15] M. A. Costa and L. L. Goncalves, J. Magn. Magn. Mater. **140-144**, 2193 (1995).
- [16] A. V. Lima, M. L. Lyra, U. M. S. Costa, J. Magn. Magn. Mater. **171**, 329 (1997).
- [17] K. Minami, J. Magn. Magn. Mater. **177-181**, 165 (1998).
- [18] T. Klotz and S. Kobe, J. Magn. Magn. Mater. **177-181**, 1359 (1998).
- [19] F. Family and T. Vicsek, Dynamics of Fractal Surfaces, World Scientific, Singapore (1991).
- [20] A. Bunde and S. Havlin (Eds.), Fractals and Disordered Media, Springer-Verlag, Heidelberg (1991).
- [21] A. Bunde and S. Havlin (Eds.), Fractals in Science, Springer-Verlag, Heidelberg (1995).
- [22] A.L. Barabasi and H.E. Stanley, Fractal Concepts in Surface Growth, Cambridge University Press, New York (1995).
- [23] M. Marsili, A. Maritan, F. Toigo, and J.R. Banavar, Rev. Mod. Phys. **68**, 963 (1996).
- [24] M. Eden, in “Symp. on Information Theory in Biology”, H.P. Yockey (Ed.), Pergamon Press, New York (1958); “Proceedings of the Fourth Berkeley Symposium on Mathematics, Statistics and Probability”, F. Neyman (Ed.), University of California Press, Berkeley, Vol.IV, p.223 (1961).
- [25] U. Bovensiepen et al., Phys. Rev. Lett. **81**, 2368 (1998).
- [26] U. Steiner, E. Eiser, J. Klein, A. Budkowski, and L.J. Fetters, Science **258**, 1126 (1992).
- [27] A. Budkowski, U. Steiner, J. Klein, and G. Schatz, Europhys. Lett. **18**, 705 (1992).
- [28] U. Steiner and J. Klein, Phys. Rev. Lett. **77**, 2526 (1996).
- [29] P. Taborek and J.E. Rutledge, Phys. Rev. Lett. **68**, 2184 (1992).
- [30] K.S. Ketola, S. Wang, and R.B. Hallock, Phys. Rev. Lett. **68**, 201 (1992).
- [31] A.F.G. Wyatt, J. Klier, and P. Stefanyi, Phys. Rev. Lett. **74**, 1151 (1995).

- [32] H.K. Christenson, Phys. Rev. Lett. **73**, 182 (1994).
- [33] A.O. Parry and R. Evans, Phys. Rev. Lett. **64**, 439 (1990); Physica A **181**, 250 (1992).
- [34] M.R. Swift, A.L. Owczarek, and J.O. Indekeu, Europhys. Lett. **14**, 465 (1991).
- [35] A. Maciolek and J. Stecki, Phys. Rev. B **54**, 1128 (1996).
- [36] A. Maciolek, J. Phys. A (Math. and Gen.) **29**, 3837 (1996).
- [37] E. Carlon and A. Drzewiński, Phys. Rev. E **57**, 2626 (1998).
- [38] H.L. Frisch, S. Puri, and P. Niebala, J. Chem. Phys. **110**, 10514 (1999).
- [39] H. Liu, A. Bhattacharya, and A. Chakrabarti, J. Chem. Phys. **109**, 8607 (1998).
- [40] M. Mueller, E.V. Albano, and K. Binder, Phys. Rev. E **62**, 5281 (2000).
- [41] K. Binder, D.P. Landau, and A.M. Ferrenberg, Phys. Rev. Lett. **74**, 298 (1995); Phys. Rev. E **51**, 2823 (1995).
- [42] K. Binder, D.P. Landau, and A.M. Ferrenberg, Phys. Rev. E **53**, 5023 (1995).
- [43] A. Wener, F. Schmid, M. Mueller, and K. Binder, J. Chem. Phys. **107**, 8175 (1997).
- [44] A.M. Ferrenberg, D.P. Landau, and K. Binder, Phys. Rev. E **58**, 3353 (1998).
- [45] M. Ausloos, N. Vandewalle, and R. Cloots, Europhys. Lett. **24**, 629 (1993); N. Vandewalle and M. Ausloos, Phys. Rev. E **50**, R635 (1994).
- [46] J. Candia and E. V. Albano, Phys. Rev. E **63**, 066127 (2001).
- [47] J. Candia and E. V. Albano, Phys. Rev. Lett. **88**, 016103 (2002); J. Phys.: Cond. Matter **14**, 4927 (2002).
- [48] K. Binder and D.W. Heermann, in Monte Carlo Simulation in Statistical Physics, Springer Series in Solid State Sciences 80, Springer-Verlag, Berlin (1992).
- [49] K. Binder and D. Stauffer, A simple introduction to Monte Carlo simulation and some specialized topics, in Applications of the Monte Carlo Method in Statistical Physics (2nd Ed.), K. Binder (Ed.), Springer-Verlag, Berlin (1987).
- [50] K. Binder, Monte Carlo Methods, in Encyclopedia of Appl. Phys., VCH Publishers Inc., Heidelberg, Vol. 10, 567 (1994).

- [51] K. Binder, Introduction to Monte Carlo Methods, Chapter 5, p.124, in Conference Proceedings Vol. 49, Monte Carlo and Molecular Dynamics of Condensed Matter Systems, K. Binder and G. Ciccotti (Eds.), SIF, Bologna (1996).
- [52] K. Binder, Z. Phys. B **43**, 119 (1981).
- [53] A.D. Bruce, J. Phys. C **14**, 3667 (1981).
- [54] M.M. Tsy-pin and H.W.J. Blöte, Phys. Rev. E **62**, 73 (2000).
- [55] L.D. Landau and E.M. Lifshitz, Statistical Physics, 3rd Edition, Part 1, Pergamon Press, Oxford (1980).
- [56] Notice that, according to the definitions given by Eqs.(3) and (4), we have used $P_L(m)$ and $P_L(M)$ for the MEM and the Ising model, respectively.
- [57] R.J. Baxter, Exactly Solved Models in Statistical Mechanics, Academic Press (1982).
- [58] M.N. Barber, in “Phase transitions and critical phenomena”, C. Domb and J.L. Lebowitz (Eds.), Academic, New York, Vol. 8, p. 146 (1983).
- [59] V. Privman (Ed.), Finite size scaling and numerical simulations of statistical systems, World Scientific, Singapore (1990).